Naval Research Laboratory
Washington, DC 20375-5000

NRL Memorandum Report 6701

Early Time Structuring of VHANES: Preliminary Results

J. D. HUBA

Space Plasma Branch
Plasma Physics Division

August 15, 1990

REPORT DOCUMENTATION PAGE

Form Approved
OMB No. 0704-0188

1. AGENCY USE ONLY *(Leave blank)*	2. REPORT DATE	3. REPORT TYPE AND DATES COVERED
	1990 August 15	Interim

4. TITLE AND SUBTITLE
Early Time Structuring of VHANES: Preliminary Results

5. FUNDING NUMBERS
47-0889-09
Work Unit Code: 00166
MIPR: 89-526

6. AUTHOR(S)
J.D. Huba

7. PERFORMING ORGANIZATION NAME(S) AND ADDRESS(ES)
Naval Research Laboratory
Code 4780.1JH
Washington, DC 20375-5000

8. PERFORMING ORGANIZATION REPORT NUMBER
NRL Memorandum Report 6701

9. SPONSORING/MONITORING AGENCY NAME(S) AND ADDRESS(ES)
Defense Nuclear Agency
Alexandria, VA 22310-3398

10. SPONSORING/MONITORING AGENCY REPORT NUMBER

11. SUPPLEMENTARY NOTES

12a. DISTRIBUTION/AVAILABILITY STATEMENT
Approved for public release; distribution unlimited.

12b. DISTRIBUTION CODE

13. ABSTRACT *(Maximum 200 words)*

The stability of the debris shell of a nuclear burst at altitudes above 400 km is investigated. A set of relatively simple expressions are derived to estimate the effective gravitational acceleration associated with the deceleration of the shell (by mass pick-up and magnetic field sweep-up) and the curvature of the magnetic field. We then present a stability analysis, based on the recent kinetic theory, developed by Huba et al. (1990). In particular, the turn-on conditions for the unmagnetized ion Rayleigh-Taylor instability are derived for both the fluid and kinetic regimes, as well as the finite Larmor radius stabilization criterion for the magnetized ion Rayleigh-Taylor instability. We apply these results to 1 MT bursts at altitudes h = 400 km, 1,000 km, and 10,000 km. We find the burst at 400 km is stable to the unmagnetized ion Rayleigh-Taylor instability; the burst at 1,000 km is marginally unstable to the kinetic instability; and the burst at 10,000 km is strongly unstable to both the kinetic and fluid instabilities. A critical parameter in determining the stability properties of the debris shell is the density gradient scale length (or shell thickness).

14. SUBJECT TERMS	15. NUMBER OF PAGES
HANE Structure, Early Time Structure, VHANE, Debris Jetting	31
	16. PRICE CODE

17. SECURITY CLASSIFICATION OF REPORT	18. SECURITY CLASSIFICATION OF THIS PAGE	19. SECURITY CLASSIFICATION OF ABSTRACT	20. LIMITATION OF ABSTRACT
Unclassified	Unclassified	Unclassified	SAR

CONTENTS

I. INTRODUCTION 1

II. DECELERATION MODELS 3

A. Mass Pick-up 3
B. Magnetic Deceleration 4
C. Curvature Acceleration 5
1. Super-Alfvénic Expansions 5
2. Sub-Alfvénic Expansions 6
D. Quantitative Results 6

III. STABILITY THEORY 7

A. Equilibrium 7
B. Dispersion Equation 8
1. High Frequency Limit ($\omega >> \Omega_i$) 9
2. Low Frequency Limit ($\omega >> \Omega_i$) 12

IV. APPLICATION TO VHANES 13

V. DISCUSSION 15

ACKNOWLEDGMENTS 16

REFERENCES 17

DISTRIBUTION LIST 23

EARLY TIME STRUCTURING OF VHANES: PRELIMINARY RESULTS

I. INTRODUCTION

An outstanding problem in the DNA HANE community is understanding the generation, evolution, and decay of plasma irregularities associated with high altitude nuclear bursts. Although the focus of this program has been on late time structure (e.g., the determination of the freezing scale size), an important aspect of the problem is early time structure. It is known that structuring does occur at very early times in HANEs ($t \lesssim$ sec); however, the exact structuring mechanisms are not well understood, nor is the impact of early time structure on late time structure known. For example, does the early time structure act as a seed mechanism for late time structure? Are the scale lengths of late time structure influenced by the early time structure? Aside from structure questions, there is also the possibility that early time structure can lead to the transport of debris across magnetic field lines; for example, weapon debris may reach much higher altitudes than expected.

Most of the research on early time stucturing has focussed on bursts which are super-Alfvénic, i.e., Starfish or Checkmate. For the purposes of discussion we will assume that the transition altitude for super-Alfvénic to sub-Alfvénic bursts occurs at h ~ 1000 km. The actual height, of course, depends upon ionospheric conditions at the time of burst (i.e., the ambient Alfvén velocity V_{Aa}) and the initial expansion velocity of the debris (i.e., V_{d0}). We will refer to sub-Alfvénic bursts as VHANEs (Very High Altitude Nuclear Explosions) since they occur for h > 1000 km.

The initial work on early time structuring was done by Brecht and Papadopoulos (1979) who suggested that a Rayleigh-Taylor instability can initiate cross-field jetting of energetic ions. Their analysis is based upon the usual MHD assumptions, i.e., $\partial/\partial t \ll \Omega_i$ and $\rho_i \ll R, L_n$: time scales small compare to the ion cyclotron period, and length scales large compared to the ion Larmor radius. They argued that the instability can be driven by (1) laminar acceleration of a group of ions within the debris-air shock, and/or (2) the centripetal force associated with the curved magnetic field. For parameters relevant to Starfish they find that the instability has a growth rate $\gamma \sim 71$ sec^{-1} (or growth time $\tau_g \sim 14$ msec) and a transverse wavelength in the range 3-30 km. However, their analysis is not entirely applicable to VHANEs (bursts at altitudes h > 1000 km) because

Manuscript approved April 26, 1990.

their results are based on relationships appropriate for super-Alfvénic plasma expansions. For example, they assume a highly compressed magnetic field in the debris-air coupling shell, and neglect the deceleration of the debris shell caused by the 'sweep-up' of the ambient magnetic field. These considerations are reasonable for super-Alfvénic bursts; however, they are not valid for sub-Alfvénic bursts. Moreover, recent theoretical work at NRL on the structuring of sub-Alfvénic plasma expansions [e.g., AMPTE magnetotail release (Bernhardt et al., 1987) and the NRL laser experiment (Ripin et al., 1987)] has found that conventional MHD theory is not valid, and that a modified MHD theory must be used which includes the Hall current (Hassam and Huba, 1987,1988; Huba et al., 1987, 1989). Of course, hybrid codes (Thomas and Brecht, 1988) and particle codes (Winske, 1989) are also appropriate because they contain the proper ion dynamics.

Very recently, Sperling (1989) has argued that the unmagnetized ion Rayleigh-Taylor instability (or the large Larmor radius instability as referred to in the NRL laser experiment) is not relevant to VHANEs. A key argument in this paper is that the conventional Rayleigh-Taylor growth rate is less than the ion cyclotron frequency (i.e., $\gamma_0 = (g/L_n)^{1/2} < \Omega_i$). First, we note that this conclusion is based only on a limited set of parameters which are poorly known. Second, and more important, we have shown in Huba et al. (1989) and in the present paper that the criterion $\gamma_0 < \Omega_i$ is overly stringent, and that a high frequency instability can occur for less stringent conditions; namely, for $\gamma_0 > (m_e/m_i)^{1/4}\Omega_i$. Thus, the modified MHD theory of Hassam and Huba (1988), and the recently developed kinetic theory of sub-Alfvénic expansions may apply to VHANEs.

The organization of the paper is as follows. In the next section we estimate the 'effective gravity' associated with HANE and VHANE plasma expansions. These results are based upon simplistic models and provide a good starting point for more detailed calculations and numerical investigations. In Section III we describe the kinetic theory of Huba et al. (1989) as it pertains to the stability of sub-Alfvénic VHANE expansions. In Section IV we apply the results of Sections II and III for bursts at altitudes h = 400 km, 1,000 km, and 10,000 km. Finally, in Section V we summarize our results.

II. DECELERATION MODELS

A. Mass Pick-up

We first estimate the deceleration of the debris-air coupling shell caused by direct momentum coupling to the background plasma. We estimate the deceleration of the shell by assuming a momentum conserving snowplow model. We assume that

$$MV_d = M_0 V_{d0} \tag{1}$$

where M is the mass, V_d is the velocity, and the subscript 0 denotes initial values. Assuming a spherical expansion we take

$$M = M_0 + \frac{4}{3}\pi R^3 n_a m_a \tag{2}$$

where R is the radius of the shell, and n_a and m_a are the density and mass of the background plasma, respectively. We substitute (2) into (1) and obtain

$$V_d = V_{d0}\left(1 + \frac{R^3}{R_M^3}\right)^{-1} \tag{3}$$

where R_M is the equal mass radius given by $R_M = (3M_o/4\pi n_a m_a)^{1/3}$. Taking the first derivative of (3) we obtain the effective gravitational acceleration g_M associated with the deceleration

$$g_M = -\frac{dV_d}{dt} = 3V_{d0}^2 \frac{R^2}{R_M^3}\left(1 + \frac{R^3}{R_M^3}\right)^{-3} \tag{4}$$

From (4) we find that the maximum inertial deceleration occurs when $R = 0.66R_M$ so that

$$g_{Mm} \simeq \frac{V_{d0}^2}{R_M} \tag{5}$$

where g_{Mm} denotes the maximum 'effective' gravity (i.e., the deceleration dV_d/dt).

B. Magnetic Deceleration

We estimate the 'stopping' radius of a magnetically confined expansion by equating the initial kinetic energy of the plasma with the magnetic energy in a volume $(4/3)\pi R_B^3$ where R_B is defined as the magnetic confinement radius,

$$\frac{1}{2} M_0 V_{d0}^2 = \frac{B_0^2}{8\pi} \left(\frac{4}{3} \pi R_B^3\right) \tag{6}$$

where M_0 is the mass of the plasma, V_{d0} is the initial debris expansion velocity, and B_0 is the ambient magnetic field. From (6) we obtain

$$R_B = \left(3M_0 V_{d0}^2 / B_0^2\right)^{1/3} \tag{7}$$

We compare this distance with the equal mass radius R_M. For the expanding plasma to be confined magnetically we require $R_B < R_M$. This leads to $V_{d0} < V_{Aa}$ where $V_{Aa} = B_0/(4\pi n_a m_a)^{1/2}$ is the Alfven velocity in the ambient plasma. When $V_{d0} << V_{Aa}$ the expanding plasma is stopped before it sweeps up very much background plasma.

We estimate g_B, the deceleration caused magnetic field sweep-up, using conservation of energy. We write

$$\frac{1}{2} M_0 V_d^2(t) + \frac{B_0^2}{8\pi} \frac{4\pi}{3} R^3(t) = \frac{1}{2} M_0 V_{d0}^2 \tag{8}$$

where the LHS of (8) is the sum of the kinetic energy of the expanding debris and the swept-up magnetic energy at time t and position R, and the RHS is the energy at t = 0. We solve (8) for $V_d(t)$ and obtain

$$V_d(t) = \left(V_{d0}^2 - \frac{B_0^2}{3M_0} R^3\right)^{1/2}. \tag{9}$$

We take the time derivative of (9) to obtain

$$g_B(t) = -\frac{dV_d}{dt} = \frac{B_0^2}{2M_0} R^2(t) = \frac{3V_{d0}^2}{2R_B} \frac{R^2}{R_B^2} \tag{10}$$

where we have made use of the fact that $V_d = dR/dt$ and the definition of

R_B. We note that the maximum deceleration occurs at $R = R_B$, the radius of maximum expansion.

C. Curvature Acceleration

1. Super-Alfvénic Expansions

We note that the curvature force is given by $F_c = B^2/4\pi R$ so that the acceleration g_C is

$$g_C = B^2/4\pi R n_T m_T \tag{11}$$

where $n_T = n_a + n_d$ and $m_T = m_a + m_d$. In the super-Alfvénic regime one can use the relationship $B^2 \sim V_d^2 4\pi n_a m_a$ (Brecht and Papdopoulos, 1979) and (3), we rewrite (11) as

$$g_C = \frac{V_{d0}^2}{R}\left(1 + \frac{R^3}{R_M^3}\right)^{-2}\left(1 + \frac{n_d m_d}{n_a m_a}\right)^{-1}. \tag{12}$$

We take $n_d m_d \gg n_a m_a$ (Clark, private communication), which is typical of Starfish for $R \lesssim R_M$, and find that (12) becomes

$$g_C = \frac{n_a m_a}{n_d m_d}\frac{V_{d0}^2}{R}\left(1 + \frac{R^3}{R_M^3}\right)^{-2} \tag{13}$$

We will assume n_a is roughly constant, but take n_d to be a decreasing function of radius as follows

$$n_d = \frac{3}{8\pi}\frac{M_0}{m_d}\frac{1}{\Delta R(3R^2 + \Delta R^2)}. \tag{14}$$

Substituting (14) into (13) we find that

$$g_C = \frac{V_{d0}^2}{R}\left(1 + \frac{R^3}{R_M^3}\right)^{-2}\frac{2\Delta R(3R^2 + \Delta R^2)}{R_M^3} \tag{15}$$

where we have made use of the definition of R_M.

2. Sub-Alfvénic Expansions

The assumptions upon which (13) is based are not valid for sub-Alfvénic expansions. In particular, the magnetic field is not compressed (i.e., the relationship $B^2 \sim V_d^2 4\pi n_a m_a$ is no longer valid) so that $B \sim B_0$ where B_0 is the ambient magnetic field. Substituting (14) into (11) we find that the curvature acceleration in the sub-Alfvénic regime is given by

$$g_C = \frac{B_0^2}{3M_0}\frac{\Delta R}{R}(3R^2 + \Delta R^2) = \frac{V_{d0}^2}{R}\frac{\Delta R}{R_B}\frac{3R^2 + \Delta R^2}{R_B^2} \qquad (16)$$

We note that g_C reaches a minimum at $R = \Delta R/\sqrt{3}$.

D. Quantitative Results

We present Fig. 1 which is a plot of g (cm/sec^2) vs. R (km) for a 1 MT burst at altitudes h = 400 km, 1,000 km, and 10,000 km. The parameters used are the following: h = 400 km [$n_a = 5.0 \times 10^5$ cm^{-3} and $m_a = 16\ m_p$ (oxygen background)]; h = 1,000 km [$n_a = 1.0 \times 10^3$ cm^{-3} and $m_a = m_p$ (hydrogen background)]; and h = 10,000 km [$n_a = 1.0$ cm^{-3} and $m_a = m_p$ (hydrogen background)]. In all cases we have taken $V_{d0} = 2.0 \times 10^8$ cm/sec, $M_0 = 5.0 \times 10^5$ gm, $m_d = 28\ m_p$ (aluminum debris), and $Z = 2$. These parameters are shown in Table I along with the relevant expansion parameters.

For h = 400 km we note that the Alfvén Mach number is $M_A = V_{d0}/V_{Aa} = 9.43$ so that $R_M < R_B$, as expected. Thus, the h = 400 km burst is super-Alfvénic; we use (4) and (15) to calculate the mass and curvature decelerations, respectively. The curvature acceleration (g_C) dominates the mass pick-up deceleration (g_M) until $R \simeq R_M/2$ where $R_M \simeq 200$ km. For $R > R_M/2$ the two accelerations are comparable. We note that the total effective gravity ($g_T = g_C + g_M$) is reasonably large throughout the expansion to R_M: $g_T \sim 10^9$ cm/sec^2.

For h = 1,000 and 10,000 km we find that the Alfvén Mach number is $M_A = 1.36 \times 10^{-1}$ and 4.71×10^{-2}, respectively. These bursts are sub-Alfvénic and therefore $R_B < R_M$. Thus, we use (10) and (16) in calculating g_B and g_C, respectively. The burst at h = 1,000 km expands to a radius $R_B \simeq 1000$ km. Early in the expansion phase we see that $g_C > g_B$ but that the magnitude of g_C is relatively small, $g_C \sim 5 \times 10^6$ cm/sec^2. Later in the

expansion phase g_B dominates over g_C and becomes reasonably large, $g_B > 10^8$ cm/sec^2. The burst at h = 10,000 km expands to a radius $R_B \simeq 5000$ km. In this situation we note that $g_B > g_C$ throughout the expansion, unlike the h = 1,000 km burst. However, the magnitude of g_B is somewhat smaller than h = 1,000 km burst; we see that $g_B > 10^7$ cm/sec^2 for R > 2000 km, reaching a maximum value $g_B \simeq 10^8$ cm/sec^2 at $R \sim R_B$. The reduction in the value of g_B as h increases is simply because the ambient magnetic field strength is decreasing, all other parameters being equal.

III. STABILITY THEORY

We now explore the stability of the expanding (and decelerating) debris plasma. A detailed kinetic theory of the stability properties of sub-Alfvénic plasma expansions in finite β, collisional plasmas has been presented in Huba et al. (1989). We will not reproduce the derivation of the dispersion equation here but refer the interested reader to Huba et al. (1989) for details.

A. Equilibrium

The plasma configuration and slab geometry used in the analysis are shown in Fig. 2. We consider a plasma with a density profile $n_0(x)$ such that $\partial n_0/\partial x < 0$; we include a magnetic field $\underset{\sim}{B} = B_0 \hat{e}_z$, an ambient electric field $\underset{\sim}{E} = -E_0 \hat{e}_x$, and a gravitational acceleration $\underset{\sim}{g} = g \hat{e}_x$. The gravitational acceleration can be associated with the transverse deceleration of a sub-Alfvénic plasma expansion in a magnetic field (i.e., $g = -d\underset{\sim}{V}_{i0}/dt$), a super-Alfvénic expansion in a background plasma, and/or the curvature acceleration, as described above. For example, in Fig. 2, one can imagine a plasma shell decelerating as it moves in the +x-direction. We also assume that the time scale of the instability is much slower than the electron cyclotron frequency (i.e., $\omega << \Omega_e$). We allow the time scale of the instability to be arbitrary in relation to the ion cyclotron period.

The electron momentum equation for this situation is given by

$$0 = \frac{e}{m_e}\left(\underset{\sim}{E}_0 + \frac{1}{c}\underset{\sim}{V}_{e0} \times \underset{\sim}{B}_0\right) - \frac{T_e}{m_e}\frac{\nabla n_0}{n_0} \quad . \tag{17}$$

From (17) it is easily shown that the equilibrium electron drift is given by

$$\underset{\sim}{V}_{e0} = (V_E + V_{de})\,\hat{e}_y \tag{18}$$

where $V_E = cE_0/B_0$ is the $\underset{\sim}{E} \times \underset{\sim}{B}$ drift velocity and $V_{de} = cT_e/eB_0L_n$ is the electron diamagnetic drift velocity where $L_n = |\partial \ln n_0/\partial x|^{-1}$.

The ion momentum equation is given by

$$0 = \frac{eZ}{m_i}\left(\underset{\sim}{E}_0 + \frac{1}{c}\underset{\sim}{V}_{i0} \times \underset{\sim}{B}_0\right) - \frac{T_i}{m_i}\frac{\nabla n_0}{n_0} + g \tag{19}$$

From (19) the equilibrium ion drift is found to be

$$\underset{\sim}{V}_{i0} = \left(\frac{cE_0}{B_0} - \frac{g}{\Omega_i} - \frac{cT_i}{eZB_0}\frac{1}{L_n}\right)\hat{e}_y \,. \tag{20}$$

The components of V_0 are the $\underset{\sim}{E} \times \underset{\sim}{B}$ drift [$V_E = cE_0/B_0$], the gravitational drift [$V_g = g/\Omega_i$], and the ion diamagnetic drift [$V_{di} = cT_i/eZB_0L_n$].

In order to satisfy the equilibrium condition $\nabla \cdot n\underset{\sim}{V}_{i0} = 0$ we choose to work in the ion rest frame, i.e., $\underset{\sim}{V}_{i0} = 0$. Thus, we take

$$\frac{cE_0}{B_0} = \frac{g}{\Omega_i} + \frac{cT_i}{eZB_0}\frac{1}{L_n} \tag{21}$$

The ions are electrostatically confined in the unmagnetized limit.

B. Dispersion Equation

For the parameters given in Table I we note β ($= 8\pi nT/B^2$) $\ll 1$, $\nu_{en} \ll \Omega_e$, and $\nu_{in} \ll \Omega_i$. Thus, we will use the low β (i.e., electrostatic), collisionless dispersion equation derived in Huba et al. (1989). In this limit the dispersion equation is

$$D(\omega,k_y) = 1 + \frac{\omega_{pe}^2}{\Omega_e^2} + \frac{2\omega_{pi}^2}{k_y^2v_i^2}(1 + i\omega G_i) + \frac{2\omega_{pe}^2}{k_y^2v_e^2}\frac{\omega_1 - \omega_2\Gamma_0(b_e)}{\omega_1} = 0 \tag{22}$$

where

$$G_i = \int_0^\infty dt\, \exp[i(\omega + k_y V_{di})t + \tfrac{1}{2}k_y^2\rho_i^2(\cos \Omega_i t - 1) + i\frac{k_y V_{di}}{\Omega_i}\sin \Omega_i t] ,$$

$\omega_1 = \omega - k_y V_E$, $\omega_2 = \omega - k_y V_E - k_y V_{de}$, $\omega_{pi}^2 = 4\pi n Z^2 e^2/m_i$, and $\omega_{pe}^2 = 4\pi n e^2/m_e$, $V_E = V_g + V_{di}$, $V_g = g/\Omega_i$, $V_{di} = cT_i/eZBL_n$, $b_e = k_y^2\rho_e^2/2$, $\mu = k_y\rho_e$, $\rho_e = v_e/\Omega_e$, $v_\alpha^2 = 2T_\alpha/m_\alpha$, $\Gamma_0(x) = \exp(-x)I_0(x)$, and $I_0(x)$ is the modified Bessel function of order 0. This dispersion equation is valid for $\omega \ll \Omega_i$, $\omega \sim \Omega_i$, and $\omega \gg \Omega_i$; thus, it describes the Rayleigh-Taylor instability in both the magnetized and unmagnetized ion limits.

1. High Frequency Limit ($\omega \gg \Omega_i$)

We first simplify (22) by considering the high frequency ($\gamma > \Omega_i$ where γ is the growth rate), short wavelength ($k_y\rho_i \gg 1$), cold electron limit ($T_e \to 0$). In this limit we note that $G_i = -i\xi_i Z(\xi_i)/\omega$ where $\xi_i = \omega/k_y v_i$, and $\Gamma_0(b_e) \simeq 1 - b_e$. The dispersion equation then becomes

$$D(\omega,k_y) = 1 + \frac{\omega_{pe}^2}{\Omega_e^2} + \frac{2\omega_{pi}^2}{k_y^2 v_i^2}(1 + \xi_i Z(\xi_i)) + \frac{2\omega_{pi}^2}{k_y^2 v_i^2}\frac{k_y V_{di}}{\omega - k_y V_E} = 0 \qquad (23)$$

We further simplify (23) by assuming the ions to be either cold ($\omega/k_y v_i \gg 1$) or warm ($\omega/k_y v_i \ll 1$), which corresponds to the strong drift velocity regime ($V_E \gg v_i$) or the weak drift velocity regime ($V_E \ll v_i$), respectively.

a. Cold Ion Limit ($\omega/k_y v_i \gg 1$)

We first consider the cold ion limit: $\omega/k_y v_i \gg 1$ [the strong drift regime (i.e., $V_E \gg v_i$)]. We expand the plasma dispersion function in (23) in its asymptotic limit. The dispersion equation then becomes

$$D(\omega,k_y) = 1 - \frac{\omega_{pi}^2}{\omega^2} + \frac{2\omega_{pi}^2}{k_y^2 v_i^2}\frac{k_y V_{di}}{\omega - k_y V_E} + \frac{\omega_{pe}^2}{\Omega_e^2} = 0 \qquad (24)$$

We can rewrite (24) in the following form

$$(\omega^2 - \omega_{lh}^2)(\omega - k_y V_E) = -\frac{\omega_{lh}^2\omega^2}{\Omega_i k_y L_n} \qquad (25)$$

where $\omega_{lh} = \omega_{pi}/(1 + \omega_{pe}^2/\Omega_e^2)^{1/2}$ is the lower hybrid frequency. Equation (25) is very similar to the dispersion equation derived by Krall and Liewer (1971) for the lower-hybrid-drift instability (see Eq. (7) of their paper); in the limit $g \to 0$ it agrees exactly with their dispersion equation. Following the analysis of Krall and Liewer (1971) one can show that the maximum growth rate of the instability is $\gamma_M \approx \omega_{lh}$ with $\omega_r \approx k_y V_E \approx \omega_{lh}$. From (25) it is clear that the instability is fluid-like and is caused by the coupling of a lower hybrid wave ($\omega = \omega_{lh}$) with a drift wave ($\omega = k_y V_E$) in an inhomogeneous plasma (i.e., finite L_n).

Equation (25) yields a relatively simple solution in the low frequency limit, i.e., $\omega << \omega_{lh}$. It is given by

$$\omega^2 - \Omega_i k_y L_N \omega + k_y^2 g L_n = 0 \tag{26}$$

where we have assumed $V_g >> V_{di}$. Equation (26) has previously been derived from fluid theory by Hassam and Huba (1987, 1988). The eigenfrequency is given by

$$\omega = \frac{1}{2}\Omega_i k_y L_n \pm \frac{1}{2}\left[(\Omega_i k_y L_n)^2 - 4 g L_n k_y^2\right]^{1/2} . \tag{27}$$

Instability occurs for $g/L_n > \Omega_i^2/4$. In the limit of large g one finds that $\gamma \approx k_y (g L_n)^{1/2}$.

b. Warm Ion Limit ($\omega/k_y v_i << 1$)

We now consider the warm ion limit: $\omega/k_y v_i << 1$ [the weak drift regime (i.e., $V_E << v_i$)]. For this situation it is found that the instability is kinetic in nature; the unstable waves grow because of inverse Landau damping of the ions. We expand the plasma dispersion function in (23) in the small argument limit. The dispersion equation then becomes

$$D(\omega, k_y) = 1 + \frac{2\omega_{pi}^2}{k_y^2 v_i^2} + \frac{2\omega_{pi}^2}{k_y^2 v_i^2}\frac{i\sqrt{\pi}\omega}{k_y v_i} + \frac{2\omega_{pi}^2}{k_y^2 v_i^2}\frac{k_y V_{di}}{\omega - k_y V_E} + \frac{\omega_{pe}^2}{\Omega_e^2} = 0 \tag{28}$$

Equation (34) can be rewritten as follows

$$0 = 1 + \frac{k_M^2}{k_y^2} + \frac{k_M^2}{k_y^2}\frac{k_y V_{di}}{\omega - k_y V_E} + \frac{k_M^2}{k_y^2}\frac{i\sqrt{\pi}\omega}{k_y v_i} \tag{29}$$

where

$$k_M^2 = \frac{2\omega_{pi}^2}{v_i^2}\left(1 + \frac{\omega_{pe}^2}{\Omega_e^2}\right)^{-1} .$$

Assuming that $\omega_r >> \gamma$, the real frequency is determined from $D(\omega_r, k_y) = 0$ and we find that

$$\omega_r = k_y V_{di}\frac{k_y^2}{k_y^2 + k_M^2} + k_y V_g . \tag{30}$$

From (30) we see that

$$\omega_r \simeq \frac{k_y^3 V_{di}}{k_M^2} + k_y V_g \qquad \text{for } k_y << k_M \tag{31a}$$

$$\omega_r \simeq k_y(V_{di} + V_g) \qquad \text{for } k_y >> k_M \tag{31b}$$

There is a significant difference in the k_y dependence of the real frequency between the ion diamagnetic drift and the gravitational drift in the long wavelength regime, $k_y << k_M$. For the case of the lower-hybrid-drift instability ($V_{di} >> V_g$) it is found that $\omega_r \propto k_y^3$, while for the unmagnetized ion Rayleigh-Taylor instability ($V_g >> V_{di}$) $\omega_r \propto k_y$.

The growth rate is determined by the expression $\gamma = -D_i(\omega_r, k_y)/(\partial D_r/\partial\omega_r)$ where the subscripts r and i refer to the real and imaginary components of D, respectively. We find that

$$\gamma = \sqrt{\pi}\left(\frac{k_M^2}{k_y^2 + k_M^2}\right)^2\left(\frac{V_{di}}{v_i}\frac{k_y^2}{k_y^2 + k_M^2} + \frac{V_g}{v_i}\right)\frac{V_{di}}{v_i} \tag{32}$$

For the case $V_g = 0$, (30) and (32) reduce to the expressions for ω_r and γ derived in Davidson et al. (1977) for the lower-hybrid-drift

instability. It can be shown that the growth rate maximizes at $k_y = k_M$; the growth rate and real frequency at $k_y = k_M$ are given by

$$\gamma_M = \frac{\sqrt{2\pi}}{8} \frac{V_{di}^2}{v_i^2} \omega_{lh} \tag{33}$$

$$\omega_M = \frac{1}{2} k_M V_{di} \tag{34}$$

In the opposite limit, when the gravitational drift dominates (i.e., $V_g >> V_{di}$) we find that the maximum growth rate occurs at $k_y = k_M/\sqrt{3}$; the corresponding values of the growth rate and real frequency are given by

$$\gamma_M = (\frac{2\pi}{3})^{1/2} \frac{9}{16} \frac{V_g}{v_i} \frac{V_{di}}{v_i} \omega_{lh} \tag{34}$$

$$\omega_M = k_M V_g \tag{35}$$

One interesting difference between the growth rate in the strong drift limit and weak drift limit is the dependence on the density gradient scale length. In the former case we found that $\gamma \propto L_n^{1/2}$ (see (27)), while in the latter case $\gamma \propto L_n^{-1}$ (see (34)). The requirement for the unmagnetized ion Rayleigh-Taylor instability to be unstable in the kinetic regime is $\gamma > \Omega_i$; from (34) we find that the turn-on condition is roughly $g/L_n > (m_e/m_i)^{1/2}\Omega_i^2$. This criterion is considerably less stringent than that for the unmagnetized ion Rayleigh-Taylor instability in the fluid limit (i.e., $g/L_n > \Omega_i^2/4$).

2. Low Frequency Limit ($\omega << \Omega_i$)

We now consider the low frequency ($\omega << \Omega_i$), short wavelength ($k_y\rho_i << 1$) limit. In this limit we note that

$$G_i = \frac{i}{\omega} (1 + \frac{k_y V_{di}}{\omega})(1 - b_i) \tag{36}$$

and the dispersion equation becomes

$$1 + \frac{\omega_{pe}^2}{\Omega_e^2} + \frac{2\omega_{pi}^2}{k_y^2 v_i^2}\left[1 + (1 + \frac{k_y V_{di}}{\omega})(1 - b_i)\right] + \frac{2\omega_{pi}^2}{k_y^2 v_i^2}\frac{k_y V_{di}}{\omega - k_y V_E} = 0 \qquad (37)$$

where $b_i = k_y^2 \rho_i^2/2$. In the limit that $\omega_{pi}^2/\Omega_i^2 >> \omega_{pe}^2/\Omega_e^2 >> 1$ it is easily shown that (37) reduces to

$$\omega^2 - (k_y V_g + k_y V_{di})\omega + \frac{g}{L_n} = 0 \qquad (38)$$

which is the usual dispersion equation for the Rayleigh-Taylor instability in the limit of magnetized ions. In the limit $\omega >> k_y V_g$, $k_y V_{di}$, the growth rate is simply given by $\gamma = (g/L_n)^{1/2}$. The instability is stabilized when $(k_y V_g + k_y V_{di})^2 > 4g/L_n$; this is the so-called finite Larmor radius stabilization of the Rayleigh-Taylor instability (Roberts and Taylor, 1962).

IV. APPLICATION TO VHANES

We now apply the results of the stability analysis presented in Section III to the nuclear burst parameters presented in Section II. We first write down the turn-on conditions for the instabilities discussed in the previous section. We cast these conditions in terms of the growth rate of the conventional Rayleigh-Taylor instability, i.e., $\gamma_0 = (g/L_n)^{1/2}$.

Instability	Turn-on Criterion
Unmagnetized Ion Rayleigh-Taylor: Fluid Limit	$\gamma_0 > \Omega_i/2$
Unmagnetized Ion Rayleigh-Taylor: Kinetic Limit	$\gamma_0 > (m_e/m_i)^{1/4}\Omega_i$
Magnetized Ion Rayleigh-Taylor: MHD Limit	$\gamma_0 > (k_y V_g + k_y V_{di})/2$

In Fig. 3 we plot γ_0/Ω_i vs. R for the burst parameters shown in Fig. 1. In calculating γ_0 we have taken the density gradient scale length to be $L_n = 50$ km. We also indicate the turn-on values for the unmagnetized ion Rayleigh-Taylor instabilities: $\gamma_0/\Omega_i > 0.5$ the fluid mode is unstable,

and $\gamma_0/\Omega_i > 0.066$ the kinetic mode is unstable. The magnetized ion Rayleigh-Taylor instability will be unstable for sufficiently small wavenumbers (i.e., $k_y\rho_i \ll 1$). For the burst at altitude h = 400 km (Starfish), we note that $\Omega_i = \Omega_{i0}(V_{d0}/V_{Aa})(1 + R^3/R_M^3)^{-1}$ which is based on the relationship $B^2 = 4\pi n_a m_a V_d^2$. Thus, we account for the compression of the magnetic field in the debris shell which occurs in a super-Alfvenic expansion. We see that $\gamma_0/\Omega_i \lesssim 0.02$ for $R \lesssim R_M$ so that the debris shell is stable to the unmagnetized ion Rayleigh-Taylor instabilities. For the burst at h = 1,000 km we find that the kinetic instability may go unstable at $R \simeq R_B$. However, the burst at h = 10,000 km is strongly unstable to both the kinetic instability (which turns-on at R = 400 km) and the fluid instability (which turns-on at R = 4000 km).

An important consideration in the above discussion is the sensitivity of the stability criterion to the density gradient scale length. For example, if we had chosen $L_n = 5$ km for the burst at h = 400 km, then the curve γ_0/Ω_i would be increased by a factor of 3 and the kinetic instability would be unstable near $R \simeq R_M$. On the other hand, if the density gradient scale length were $L_n = 100$ km for the burst at h = 1,000 km, then the expansion would be predicted to be stable to the unmagnetized ion Rayleigh-Taylor instability. Moreover, the density gradient scale length will probably not be constant during the expansion; clearly, computer simulations are needed to better determine the thickness of the debris shell as it expands and decelerates.

Finally, we present Fig. 4 which is a plot of γ/Ω_i versus $k_y\rho_i$. We solve (22) numerically for a set of parameters relevant to the burst at h = 10,000 km at an expansion radius R = 5,000 km. We consider the following parameters: $V_g/v_i = 4.0$, $V_{di}/v_i = 0.014$, $L_n = 50$ km, $T_e/T_i = 1.0$, $T_i = T_d = T_a = 50$ ev, $\beta_i = 0.0$, $\omega_{pe}/\Omega_e = 10.0$, $Z = 2$, and $\mu_d = 28$ (aluminum). The two branches of unstable modes are apparent. In the low frequency ($\gamma < \Omega_i$), long wavelength limit ($k_y\rho_i \ll 1$) we obtain the conventional magnetized ion Rayleigh-Taylor instability; for $k_y\rho_i \ll 1$ we find that the growth rate asymptotes to the standard growth rate $\gamma_0 = (g/L_n)^{1/2} \simeq 0.335\ \Omega_i$. The local approximation breaks down for $k_y L_n \lesssim 1$ which occurs for $k_y\rho_i \simeq 0.028$ so that the results presented are valid. As $k_y\rho_i$ increases above $k_y\rho_i \sim 0.15$ we see that the mode becomes stable because of finite Larmor radius effects and the real frequency associated

with the gravitational drift wave. In the high frequency ($\gamma > \Omega_i$), short wavelength limit ($k_y \rho_i >> 1$) we find the unmagnetized ion Rayleigh-Taylor instability which is driven by a coupling between the gravitational drift wave and the lower hybrid wave. The growth rate maximizes for $\omega_r \simeq \omega_{lh}$ where $\omega_{lh} = (\Omega_e \Omega_i)^{1/2}$ is the lower hybrid frequency. For the parameters chosen, we find that the growth rate maximizes at $k_y \rho_i \simeq 40$ which corresponds to a wavelength $\lambda \simeq 200$ m. On the other hand, if we were to assume that the dominant wavelength is $\lambda \simeq L_n$, this would correspond to $k_y \rho_i \simeq 0.176$ which is stable for the parameters chosen.

We add that we have chosen a single set of parameters; based on these parameters our results suggest that the unmagnetized ion Rayleigh-Taylor instability (or the large Larmor radius instability) can play a dominant role in the structuring of the debris shell for a VHANE. However, the results are sensitive to several parameters, in particular the density gradient scale length, and simulation studies are needed to better determine the macroscopic parameters associated with a VHANE (Thomas and Brecht, 1988; Winske, 1989).

V. DISCUSSION

The stability of the debris shell of a nuclear burst at altitudes h > 400 km is investigated. A set of relatively simple expressions are derived to estimate the effective gravitational acceleration associated with the deceleration of the shell (by mass 'pick-up' and magnetic field 'sweep-up') and the curvature of the magnetic field. We then present a stability analysis based on the recent kinetic theory developed by Huba et al. (1989). In particular, the 'turn-on' conditions for the unmagnetized ion Rayleigh-Taylor instability are derived for both the fluid and kinetic regimes, as well as the finite Larmor radius stabilization criterion for the magnetized ion Rayleigh-Taylor instability. We apply these results to 1 MT bursts at altitudes h = 400 km, 1,000 km, and 10,000 km. We find the burst at h = 400 km to be stable to the unmagnetized ion Rayleigh-Taylor instability; the burst at h = 1,000 is marginally unstable to the kinetic instability; and the burst at h = 10,000 km is strongly unstable to both the kinetic and fluid unmagnetized ion Rayleigh-Taylor instabilities. On the other hand, the magnetized ion Rayleigh-Taylor instability is unstable at all altitudes and may cause structuring of the debris shell depending

on the growth rate of the instability. A critical parameter in determining the stability properties of the debris shell is the density gradient scale length (or shell thickness). It is recommended that detailed 2D and/or 3D computer simulations be performed to quantify the macroscopic parameters associated with the expansion of the debris shell (Thomas and Brecht, 1988; Winske, 1989)

ACKNOWLEDGMENTS

This research was supported by the Defense Nuclear Agency.

REFERENCES

Bernhardt, P.A., R. Roussel-Dupre, M.B. Pongratz, G. Haerendel, A. Valenzuela, D.A. Gurnett, and R.R. Anderson, "Observations and theory of the AMPTE barium releases," J. Geophys. Res., 92, 5777 (1987).

Brecht, S.H. and K. Papadopoulos, "Cross field jetting of energetic ions produced by Rayleigh-Taylor instability," NRL Memo Report 4068, 1979.

Hassam, A.B. and J.D. Huba, "Structuring of the AMPTE magnetotail barium releases," Geophys. Res. Lett., 14, 60 (1987).

Hassam, A.B. and J.D. Huba, "Magnetohydrodynamic equations for systems with large Larmor radius," Phys. Fluids, 31, 319 (1988).

Huba, J.D., J.G. Lyon, and A.B. Hassam, "Theory and simulation of the Rayleigh-Taylor instability in the limit of large Larmor radius," Phys. Rev. Lett., 59, 2971 (1987).

Huba, J.D., A.B. Hassam, and P. Satyanarayana, "Nonlocal theory of the Rayleigh-Taylor instability in the limit of unmagnetized ions," Phys. Fluids B, 1, 931 (1989).

Huba, J.D., A.B. Hassam, and D. Winske, "Stability of sub-Alfvenic expansions," to be published in Phys. Fluids B (1990).

Ripin, B.H., E.A. McLean, C.K. Manka, C. Pawley, J.A. Stamper, T.A. Peyser, A.N. Mostovych, J. Grun, A.B. Hassam, and J.D. Huba, "Large-Larmor-Radius interchange instability," Phys. Rev. Lett., 59, 2299 (1987).

Sperling, J., "The freezing-scale algorithm for both very low and very high altitudes: Physics elaboration", JAYCOR Report J201-87-1697/2547 (1989).

Thomas, V.A. and S.H. Brecht, "Early-time debris structuring and transport in a VHANE, simulations of the Rayleigh-Taylor instability," Rep. DNA-TR-88-199, Defense Nuclear Agency (1988).

Winske, D., "Development of flute modes on expanding plasma clouds," Phys. Fluids B, 1, 1900 (1989).

TABLE I: BURST PARAMETERS

	Burst Altitude h (km)		
	400	1,000	10,000
Initial expansion velocity (V_{d0})	2000 km/sec	2000 km/sec	2000 km/sec
Mass of burst (M_0)	5.0×10^5 gm	5.0×10^5 gm	5.0×10^5 gm
Ambient magnetic field (G)	0.28	0.21	0.020
Debris atomic number (μ_d)	28	28	28
Background atomic number (μ_a)	16	1	1
Ambient density (n_a)	5.0×10^5 cm^{-3}	1.0×10^3 cm^{-3}	1 cm^{-3}
Debris temperature (T_d)	50 ev	50 ev	50 ev
Debris thermal velocity (v_d)	18.5 km/sec	18.5 km/sec	18.5 km/sec
Debris charge state (Z)	2	2	2
Density gradient scale length (L_n)	50 km	50 km	50 km
Ambient cyclotron frequency (Ω_i)	188 rad/sec	146 rad/sec	13.3 rad/sec
Directed Larmor radius (V_{d0}/Ω_i)	10.6 km	13.7 km	150 km
Ambient Alfvén velocity (V_{da})	2×10^2 km/sec	2×10^4 km/sec	4×10^4 km/sec
Alfvén Mach number (M_A)	9.43	0.136	0.047
Equal mass radius (R_M)	2.0×10^2 km	4.1×10^3 km	4.1×10^4 km
Magnetic confinement radius (R_B)	9.1×10^2 km	1.1×10^3 km	5.3×10^3 km

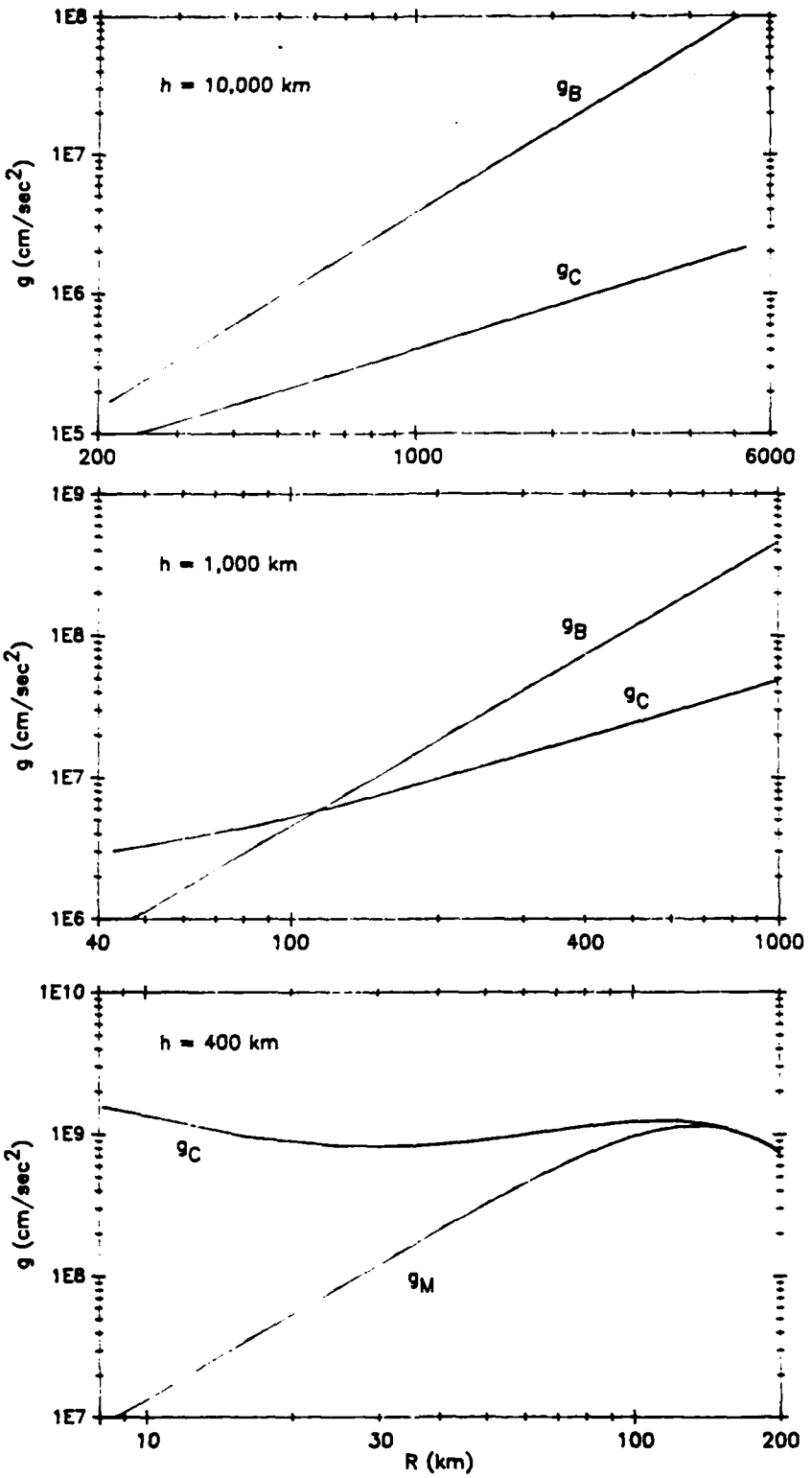

Fig. 1 — Plot of g (cm/sec^2) vs R (km) for a 1 MT burst at altitudes h = 400 km, 1,000 km, and 10,000 km. The parameters used are the following: h = 400 km [$n_a = 5.0 \times 10^5$ cm^{-3} and $m_a = 16\ m_p$ (oxygen background)]; h = 1,000 km [$n_a = 1.0 \times 10^3$ cm^{-3} and $m_a = m_p$ (hydrogen background)]; and h = 100,000 km [$n_a = 1.0$ cm$_{-3}$ and $m_a = m_p$ (hydrogen background)]. In all cases we have taken $V_{s0} = 2.0 \times 10^8$ cm/sec, $M_0 = 5.0 \times 10^5$ gm, $m_d = 28\ m_p$ (aluminum debris), and Z = 2. These parameters are shown in Table I along with the relevant expansion parameters.

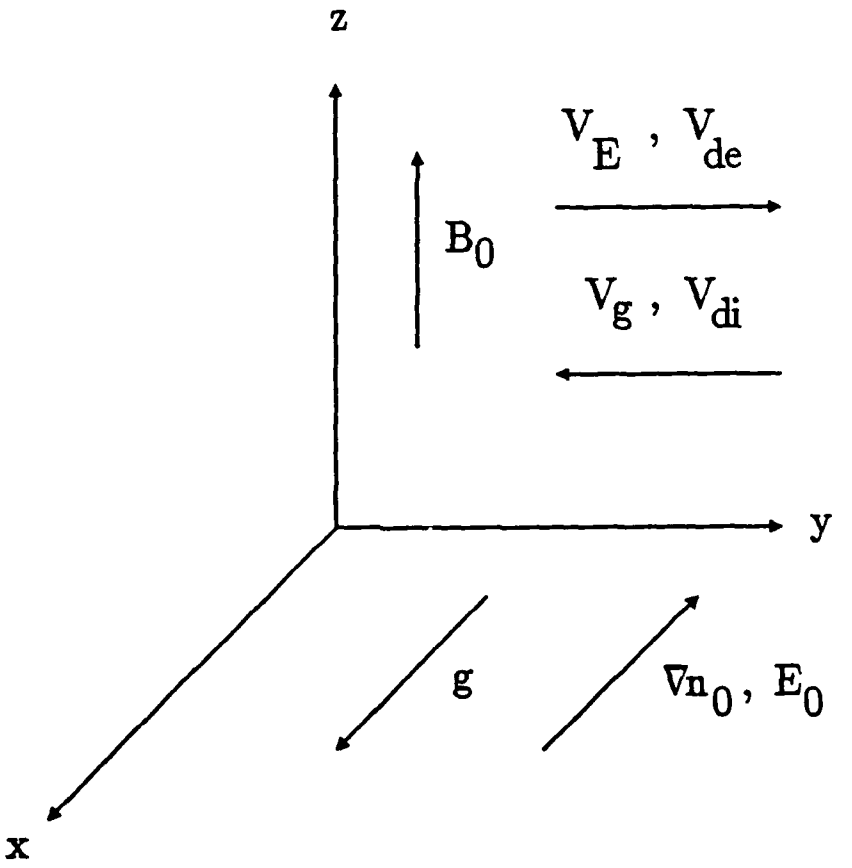

Fig. 2 — Slab geometry and plasma configuration used in the stability analysis

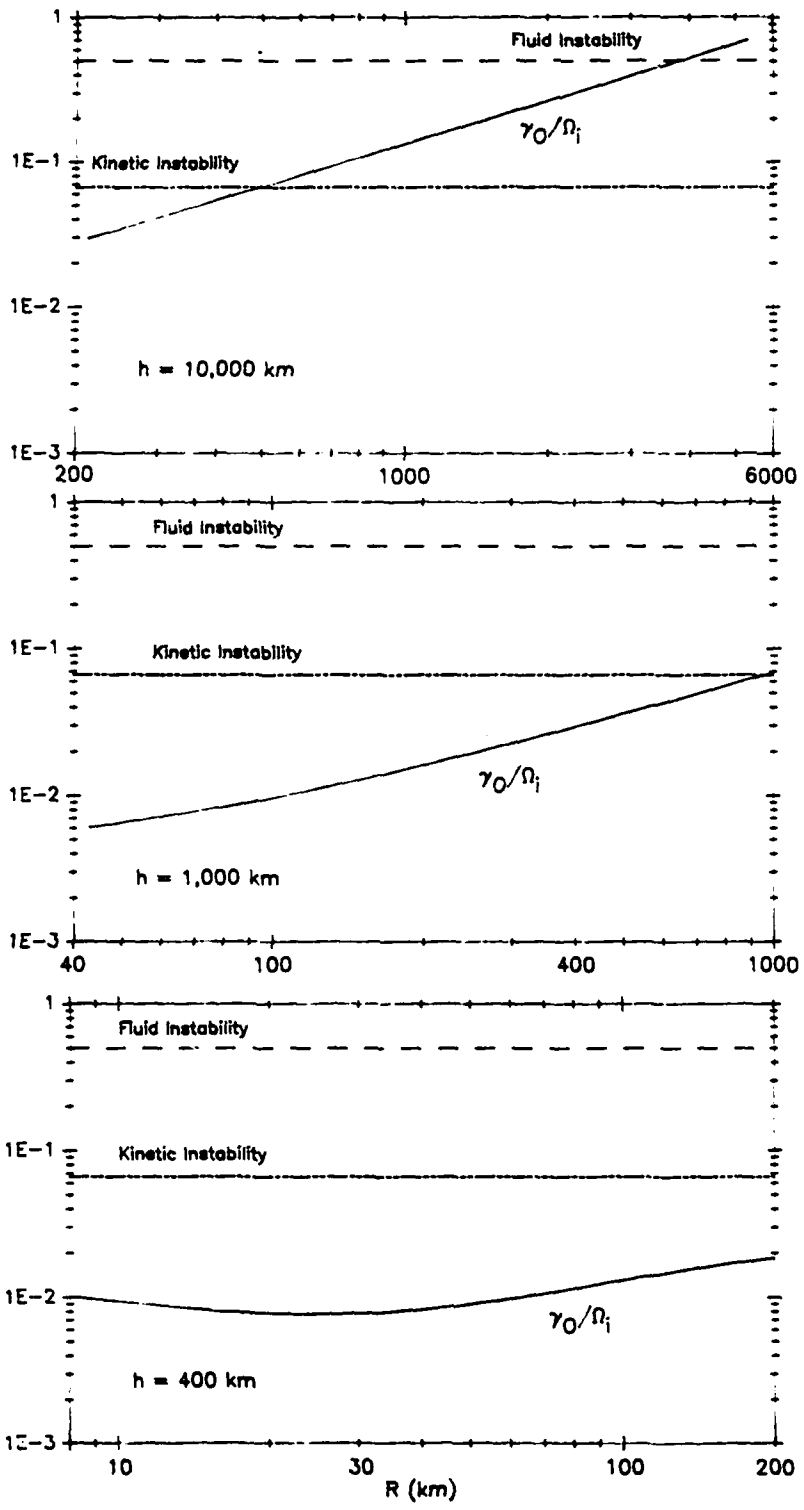

Fig. 3 — Plot of γ_0/Ω_i vs R for the burst parameters shown in Fig. 1. In calculating γ_0 we have taken the density gradient scale length to be L_n = 50 km. We also indicate the turn-on values for the unmagnetized ion Rayleigh-Taylor instabilities; $\gamma_0/\Omega_i > 0.5$ the fluid mode is unstable, and $\gamma_0/\Omega_i > 0.066$ the kinetic mode is unstable. The magnetized ion Rayleigh-Taylor instability will be unstable for sufficiently small wavenumbers (i.e., $k_y\rho_i << 1$).

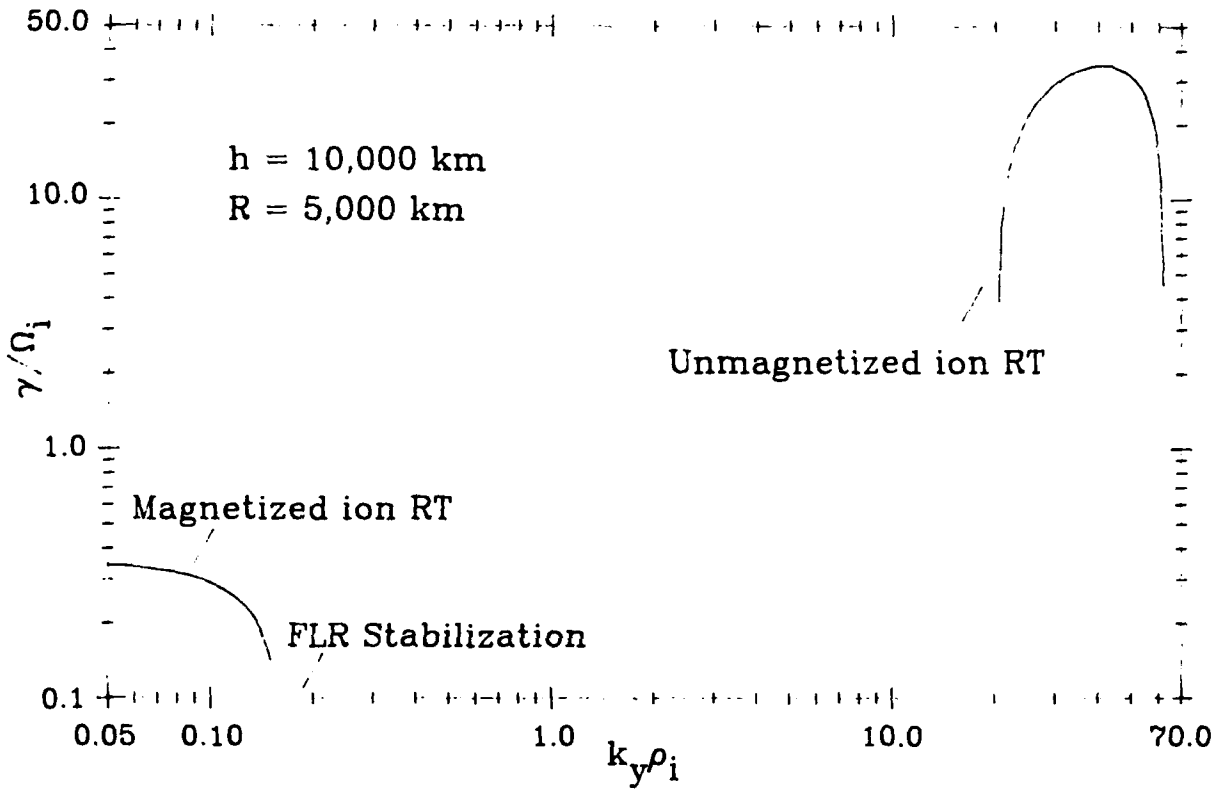

Fig. 4 — Plot of γ/Ω_i vs $k_y\rho_i$ for a set of parameters relevant to the burst at h = 10,000 km at an expansion radius R = 5,000 km. We consider the following parameters: V_g/v_i = 4.0, V_{di}/v_i = 0.014, L_n = 50 km, T_e/T_i = 1.0, $T_i = T_d = T_a$ = 50 ev, β_i = 0.0, ω_{pe}/Ω_e = 10.0, Z = 2, and μ_d = 28 (aluminum).

DISTRIBUTION LIST
(Unclassified Only)

DEPARTMENT OF DEFENSE

DIRECTOR
DEFENSE NUCLEAR AGENCY
WASHINGTON, DC 20305
04CY ATTN TITL
03CY ATTN RAAE

CHIEF
LIVERMORE DIVISION FLD COMMAND DNA
DEPARTMENT OF DEFENSE
LAWRENCE LIVERMORE LABORATORY
P.O. BOX 808
LIVERMORE, CA 94550
01CY ATTN FCPRL

COMMANDER
NAVAL OCEAN SYSTEMS CENTER
SAN DIEGO, CA 92152
01CY ATTN J. FERGUSON

NAVAL RESEARCH LABORATORY
WASHINGTON, DC 20375-5000
26CY ATTN CODE 4700/S. OSSAKOW
10CY ATTN CODE 4780/B. RIPIN
01CY ATTN CODE 4701
01CY ATTN CODE 4780.1EM/E. MCLEAN
20CY ATTN CODE 4781/4782
01CY ATTN CODE 4785
20CY ATTN CODE 2628
01CY ATTN CODE 1004/P. MANGE
01CY ATTN CODE 8344/M. KAPLAN

OFFICE OF NAVAL RESEARCH
ARLINGTON, VA 22217
01CY ATTN CODE 112S

AIR FORCE GEOPHYSICS LABORATORY
HANSCOM AFB, MA 01731
01CY ATTN OPR/HAROLD GARDNER
01CY ATTN LKB/
KENNETH S.W. CHAMPION
01CY ATTN OPR/ALVA T. STAIR
01CY ATTN PHD/JURGEN BUCHAU
01CY ATTN PHD/JOHN P. MULLEN

AF WEAPONS LABORATORY
KIRTLAND AFB, NM 87117
01CY ATTN SUL

WRIGHT AERONAUTICAL LABORATORIES
WRIGHT-PATTERSON AFB, OH 45433-6543
01CY ATTN AAAI/WADE HUNT
01CY ATTN AAAI/ALLEN JOHNSON

HEADQUARTERS
ELECTRONIC SYSTEMS DIVISION
DEPARTMENT OF THE AIR FORCE
HANSCOM AFB, MA 01731-5000
01CY ATTN J. DEAS
ESD/SCD-4

COMMANDER
ROME AIR DEVELOPMENT CENTER, AFSC
GRIFFIN AFB, NY 13441
01CY ATTN DOC LIBRARY/TSLD
01CY ATTN OCSE/V. COYNE

COMMANDER
ROME AIR DEVELOPMENT CENTER, AFSC
HANSCOM AFB, MA 01731
01CY ATTN EEP/A. LORENTZEN

UNIVERSITY OF CALIFORNIA
LAWRENCE LIVERMORE LABORATORY
P.O. BOX 808
LIVERMORE, CA 94550
01CY ATTN DOC CON FOR
TECH INFO DEPT
01CY ATTN DOC CON FOR
L-389/R. OTT
01CY ATTN DOC CON FOR
L-31/R. HAGER

LOS ALAMOS NATIONAL LABORATORY
P.O. BOX 1663
LOS ALAMOS, NM 87545
01CY ATTN J. WOLCOTT
01CY ATTN E. JONES
01CY ATTN J. MALIK
01CY ATTN R. JEFFRIES
01CY ATTN J. ZINN
01CY ATTN D. WESTERVELT
01CY ATTN D. SAPPENFIELD

LOS ALAMOS NATIONAL LABORATORY
MS D438
LOS ALAMOS, NM 87545
01CY ATTN S.P. GARY
01CY ATTN J. BOROVSKY

LOS ALAMOS NATIONAL LABORATORY
MS E531
LOS ALAMOS, NM 87545
01CY ATTN D. WINSKE
01CY ATTN V. THOMAS

SANDIA LABORATORIES
P.O. BOX 5800
ALBUQUERQUE, NM 87115
01CY ATTN W. BROWN
01CY ATTN A. THORNBROUGH
01CY ATTN T. WRIGHT
01CY ATTN D. DAHLGREN
01CY ATTN 3141
01CY ATTN SPACE PROJ DIV

SANDIA LABORATORIES
LIVERMORE LABORATORY
P.O. BOX 969
LIVERMORE, CA 94550
01CY ATTN B. MURPHEY
01CY ATTN T. COOK

NATL. OCEANIC & ATMOSPHERIC
ADMINISTRATION
ENVIRONMENTAL RESEARCH LABS
DEPARTMENT OF COMMERCE
BOULDER, CO 80302
01CY ATTN R. GRUBB

DEPARTMENT OF DEFENSE CONTRACTORS

AUSTIN RESEARCH ASSOCIATION, INC.
1901 RUTLAND DRIVE
AUSTIN, TX 78758
01CY ATTN L. SLOAN
01CY ATTN R. THOMPSON

BERKELEY RESEARCH ASSOCIATES, INC.
P.O. BOX 983
BERKELEY, CA 94701
01CY ATTN J. WORKMAN
01CY ATTN C. PRETTIE
01CY ATTN S. BRECHT
01CY ATTN N. T. GLADD

EOS TECHNOLOGIES, INC.
606 WILSHIRE BLVD.
SANTA MONICA, CA 90401
01CY ATTN C.G. GABBARD
01CY ATTN R. LELEVIER

GEOPHYSICAL INSTITUTE
UNIVERSITY OF ALASKA
FAIRBANKS, AK 99701
01CY ATTN SECURITY OFFICER
01CY ATTN T.N. DAVIS
01CY ATTN NEAL BROWN

INSTITUTE FOR DEFENSE ANALYSIS
1801 NO. BEAUREGARD STREET
ALEXANDRIA, VA 22311
01CY ATTN ERNEST BAUER
01CY ATTN HANS WOLFARD

JAYCOR
P.O. BOX 85154
11011 TORREYANA ROAD
SAN DIEGO, CA 92138
01CY ATTN J.L. SPERLING
01CY ATTN C. CHU

JOHNS HOPKINS UNIVERSITY
APPLIED PHYSICS LABORATORY
JOHNS HOPKINS ROAD
LAUREL, MD 20810
01CY ATTN DOC LIBRARIAN
01CY ATTN THOMAS POTEMRA
01CY ATTN JOHN DASSOULAS

KAMAN SCIENCES CORPORATION
P.O. BOX 7463
COLORADO SPRINGS, CO 80933
01CY ATTN T. MEAGHER

KAMAN TEMPO-CENTER FOR ADVANCED
STUDIES
816 STATE STREET
(P.O. DRAWER QQ)
SANTA BARBARA, CA 93102
01CY ATTN DASIAC
01CY ATTN WARREN S. KNAPP
01CY ATTN WILLIAM MCNAMARA
01CY ATTN B. GAMBILL

MISSION RESEARCH CORPORATION
735 STATE STREET
SANTA BARBARA, CA 03101
01CY ATTN P. FISCHER
01CY ATTN W.F. CREVIER
01CY ATTN STEVEN L. GUTSCHE
01CY ATTN R. BOGUSCH
01CY ATTN R. HENDRICK
01CY ATTN RALPH KILB
01CY ATTN DAVE SOWLE
01CY ATTN F. FAJEN
01CY ATTN M. SCHEIBE
01CY ATTN CONRAD L. LONGMIRE
01CY ATTN B. WHITE
01CY ATTN R. STAGAT
01CY ATTN D. KNEPP
01CY ATTN C. RINO

MISSION RESEARCH CORPORATION
1720 RANDOLPH ROAD, S.E.
ALBUQUERQUE, NM 87106
01CY ATTN R. STELLINGWERF
01CY ATTN M. ALME
01CY ATTN L. WRIGHT

RUTGERS UNIVERSITY
DEPT. OF MECHANICAL & AEROSPACE
ENGINEERING
P.O. BOX 909
PISCATAWAY, NJ 08855-0909
01CY ATTN PROF. NORMAN J. ZABUSKY

DEPT
PACIFIC-SIERRA RESEARCH CORP
12340 SANTA MONICA BLVD
LOS ANGELES, CA 90025
01CY ATTN E.C. FIELD, JR

PENNSYLVANIA STATE UNIVERSITY
IONOSPHERE RESEARCH LAB
318 ELECTRICAL ENGINEERING EAST
UNIVERSITY PARK, PA 16802
UNIVERSITY PARK, PA 16802
01 CY ATTN IONOSPHERIC
RESEARCH LAB

PHOTOMETRICS, INC.
4 ARROW DRIVE
WOBURN, MA 01801
01CY ATTN IRVING L. KOFSKY

R & D ASSOCIATES
P.O. BOX 9695
MARINA DEL REY, CA 90291
01CY ATTN FORREST GILMORE
01CY ATTN W.B. WRIGHT, JR
01CY ATTN W.J. KARZAS
01CY ATTN H. ORY
01CY ATTN C. MACDONALD
01CY ATTN BRIAN LAMB
01CY ATTN MORGAN GROVER

SRI INTERNATIONAL
333 RAVENSWOOD AVENUE
MENLO PARK, CA 94025
01CY ATTN J. CASPER
01CY ATTN DONALD NEILSON
01CY ATTN G. SMITH
01CY ATTN R. TSUNODA
01CY ATTN D.A. JOHNSON
01CY ATTN W.G. CHESNUT
01CY ATTN WALTER JAYE
01CY ATTN J. VICKREY
01CY ATTN G. CARPENTER
01CY ATTN G. PRICE
01CY ATTN R. LIVINGSTON
01CY ATTN V. GONZALES

DISTRIBUTION LIST
(Unclassified Only)

DEPARTMENT OF DEFENSE

DIRECTOR
DEFENSE NUCLEAR AGENCY
WASHINGTON, DC 20305
04CY ATTN TITL
03CY ATTN RAAE

CHIEF
LIVERMORE DIVISION FLD COMMAND DNA
DEPARTMENT OF DEFENSE
LAWRENCE LIVERMORE LABORATORY
P.O. BOX 808
LIVERMORE, CA 94550
01CY ATTN FCPRL

COMMANDER
NAVAL OCEAN SYSTEMS CENTER
SAN DIEGO, CA 92152
01CY ATTN J. FERGUSON

NAVAL RESEARCH LABORATORY
WASHINGTON, DC 20375-5000
26CY ATTN CODE 4700/S. OSSAKOW
10CY ATTN CODE 4780/B. RIPIN
01CY ATTN CODE 4701
01CY ATTN CODE 4780.1EM/E. MCLEAN
20CY ATTN CODE 4781/4782
01CY ATTN CODE 4785
20CY ATTN CODE 2628
01CY ATTN CODE 1004/P. MANGE
01CY ATTN CODE 8344/M. KAPLAN

OFFICE OF NAVAL RESEARCH
ARLINGTON, VA 22217
01CY ATTN CODE 112S

AIR FORCE GEOPHYSICS LABORATORY
HANSCOM AFB, MA 01731
01CY ATTN OPR/HAROLD GARDNER
01CY ATTN LKB/
KENNETH S.W. CHAMPION
01CY ATTN OPR/ALVA T. STAIR
01CY ATTN PHD/JURGEN BUCHAU
01CY ATTN PHD/JOHN P. MULLEN

AF WEAPONS LABORATORY
KIRTLAND AFB, NM 87117
01CY ATTN SUL

WRIGHT AERONAUTICAL LABORATORIES
WRIGHT-PATTERSON AFB, OH 45433-6543
01CY ATTN AAAI/WADE HUNT
01CY ATTN AAAI/ALLEN JOHNSON

HEADQUARTERS
ELECTRONIC SYSTEMS DIVISION
DEPARTMENT OF THE AIR FORCE
HANSCOM AFB, MA 01731-5000
01CY ATTN J. DEAS
ESD/SCD-4

COMMANDER
ROME AIR DEVELOPMENT CENTER, AFSC
GRIFFIN AFB, NY 13441
01CY ATTN DOC LIBRARY/TSLD
01CY ATTN OCSE/V. COYNE

COMMANDER
ROME AIR DEVELOPMENT CENTER, AFSC
HANSCOM AFB, MA 01731
01CY ATTN EEP/A. LORENTZEN

UNIVERSITY OF CALIFORNIA
LAWRENCE LIVERMORE LABORATORY
P.O. BOX 808
LIVERMORE, CA 94550
01CY ATTN DOC CON FOR
TECH INFO DEPT
01CY ATTN DOC CON FOR
L-389/R. OTT
01CY ATTN DOC CON FOR
L-31/R. HAGER

LOS ALAMOS NATIONAL LABORATORY
P.O. BOX 1663
LOS ALAMOS, NM 87545
01CY ATTN J. WOLCOTT
01CY ATTN E. JONES
01CY ATTN J. MALIK
01CY ATTN R. JEFFRIES
01CY ATTN J. ZINN
01CY ATTN D. WESTERVELT
01CY ATTN D. SAPPENFIELD

LOS ALAMOS NATIONAL LABORATORY
MS D438
LOS ALAMOS, NM 87545
01CY ATTN S.P. GARY
01CY ATTN J. BOROVSKY

LOS ALAMOS NATIONAL LABORATORY
MS E531
LOS ALAMOS, NM 87545
01CY ATTN D. WINSKE
01CY ATTN V. THOMAS

SANDIA LABORATORIES
P.O. BOX 5800
ALBUQUERQUE, NM 87115
01CY ATTN W. BROWN
01CY ATTN A. THORNBROUGH
01CY ATTN T. WRIGHT
01CY ATTN D. DAHLGREN
01CY ATTN 3141
01CY ATTN SPACE PROJ DIV

SANDIA LABORATORIES
LIVERMORE LABORATORY
P.O. BOX 969
LIVERMORE, CA 94550
01CY ATTN B. MURPHEY
01CY ATTN T. COOK

NATL. OCEANIC & ATMOSPHERIC ADMINISTRATION
ENVIRONMENTAL RESEARCH LABS
DEPARTMENT OF COMMERCE
BOULDER, CO 80302
01CY ATTN R. GRUBB

DEPARTMENT OF DEFENSE CONTRACTORS

AUSTIN RESEARCH ASSOCIATION, INC.
1901 RUTLAND DRIVE
AUSTIN, TX 78758
01CY ATTN L. SLOAN
01CY ATTN R. THOMPSON

BERKELEY RESEARCH ASSOCIATES, INC.
P.O. BOX 983
BERKELEY, CA 94701
01CY ATTN J. WORKMAN
01CY ATTN C. PRETTIE
01CY ATTN S. BRECHT
01CY ATTN N. T. GLADD

EOS TECHNOLOGIES, INC.
606 WILSHIRE BLVD.
SANTA MONICA, CA 90401
01CY ATTN C.G. GABBARD
01CY ATTN R. LELEVIER

GEOPHYSICAL INSTITUTE
UNIVERSITY OF ALASKA
FAIRBANKS, AK 99701
01CY ATTN SECURITY OFFICER
01CY ATTN T.N. DAVIS
01CY ATTN NEAL BROWN

INSTITUTE FOR DEFENSE ANALYSIS
1801 NO. BEAUREGARD STREET
ALEXANDRIA, VA 22311
01CY ATTN ERNEST BAUER
01CY ATTN HANS WOLFARD

JAYCOR
P.O. BOX 85154
11011 TORREYANA ROAD
SAN DIEGO, CA 92138
01CY ATTN J.L. SPERLING
01CY ATTN C. CHU

JOHNS HOPKINS UNIVERSITY
APPLIED PHYSICS LABORATORY
JOHNS HOPKINS ROAD
LAUREL, MD 20810
01CY ATTN DOC LIBRARIAN
01CY ATTN THOMAS POTEMRA
01CY ATTN JOHN DASSOULAS

KAMAN SCIENCES CORPORATION
P.O. BOX 7463
COLORADO SPRINGS, CO 80933
01CY ATTN T. MEAGHER

KAMAN TEMPO-CENTER FOR ADVANCED STUDIES
816 STATE STREET
(P.O. DRAWER QQ)
SANTA BARBARA, CA 93102
01CY ATTN DASIAC
01CY ATTN WARREN S. KNAPP
01CY ATTN WILLIAM MCNAMARA
01CY ATTN B. GAMBILL

MISSION RESEARCH CORPORATION
735 STATE STREET
SANTA BARBARA, CA 03101
01CY ATTN P. FISCHER
01CY ATTN W.F. CREVIER
01CY ATTN STEVEN L. GUTSCHE
01CY ATTN R. BOGUSCH
01CY ATTN R. HENDRICK
01CY ATTN RALPH KILB
01CY ATTN DAVE SOWLE
01CY ATTN F. FAJEN
01CY ATTN M. SCHEIBE
01CY ATTN CONRAD L. LONGMIRE
01CY ATTN B. WHITE
01CY ATTN R. STAGAT
01CY ATTN D. KNEPP
01CY ATTN C. RINO

MISSION RESEARCH CORPORATION
1720 RANDOLPH ROAD, S.E.
ALBUQUERQUE, NM 87106
01CY ATTN R. STELLINGWERF
01CY ATTN M. ALME
01CY ATTN L. WRIGHT

RUTGERS UNIVERSITY
DEPT. OF MECHANICAL & AEROSPACE
ENGINEERING
P.O. BOX 909
PISCATAWAY, NJ 08855-0909
01CY ATTN PROF. NORMAN J. ZABUSKY

DEPT
PACIFIC-SIERRA RESEARCH CORP
12340 SANTA MONICA BLVD
LOS ANGELES, CA 90025
01CY ATTN E.C. FIELD, JR

PENNSYLVANIA STATE UNIVERSITY
IONOSPHERE RESEARCH LAB
318 ELECTRICAL ENGINEERING EAST
UNIVERSITY PARK, PA 16802
UNIVERSITY PARK, PA 16802
01 CY ATTN IONOSPHERIC
RESEARCH LAB

PHOTOMETRICS, INC.
4 ARROW DRIVE
WOBURN, MA 01801
01CY ATTN IRVING L. KOFSKY

R & D ASSOCIATES
P.O. BOX 9695
MARINA DEL REY, CA 90291
01CY ATTN FORREST GILMORE
01CY ATTN W.B. WRIGHT, JR
01CY ATTN W.J. KARZAS
01CY ATTN H. ORY
01CY ATTN C. MACDONALD
01CY ATTN BRIAN LAMB
01CY ATTN MORGAN GROVER

SRI INTERNATIONAL
333 RAVENSWOOD AVENUE
MENLO PARK, CA 94025
01CY ATTN J. CASPER
01CY ATTN DONALD NEILSON
01CY ATTN G. SMITH
01CY ATTN R. TSUNODA
01CY ATTN D.A. JOHNSON
01CY ATTN W.G. CHESNUT
01CY ATTN WALTER JAYE
01CY ATTN J. VICKREY
01CY ATTN G. CARPENTER
01CY ATTN G. PRICE
01CY ATTN R. LIVINGSTON
01CY ATTN V. GONZALES

Do NOT make labels for
Records ----(01 cy)
Code 4827 --(22 cys)

Director of Research
U.S. Naval Academy
Annapolis, MD 21402
(2 copies)

Naval Research Laboratory
Washington, DC 20375-5000
Code 4830
Timothy Calderwood

Naval Research Laboratory
Washington, DC 20375-5000
Code 1220